Bayesian determination of the effect of a deep eutectic solvent on the structure of lipid monolayers

A. R. McCluskey,[1, 2, *] A. Sanchez-Fernandez,[1, 3, †] K. J. Edler,[1]
S. C. Parker,[1] A. J. Jackson,[3, 4] R. A. Campbell,[5, 6] and T. Arnold[1, 2, 3, 7, ‡]

[1]*Department of Chemistry, University of Bath, Claverton Down, Bath, BA2 7AY, UK*
[2]*Diamond Light Source, Harwell Campus, Didcot, OX11 0DE, UK*
[3]*European Spallation Source, SE-211 00 Lund, Sweden*
[4]*Department of Physical Chemistry, Lund University, SE-211 00 Lund, Sweden*
[5]*Division of Pharmacy and Optometry, University of Manchester, Manchester, UK*
[6]*Institut Laue-Langevin, 71 avenue des Martyrs, 38000, Grenoble, France*
[7]*ISIS Neutron and Muon Source, Science and Technology Facilities Council,*
Rutherford Appleton Laboratory, Harwell Oxford, Didcot, OX11 0QX, UK
(Dated: January 11, 2019)

In this work, we present the first example of the self-assembly of phospholipid monolayers at the interface between air and an ionic solvent. Deep eutectic solvents are a novel class of environmentally friendly non-aqueous room temperature liquids with tunable properties, that have wide ranging potential applications and are capable of promoting the self-assembly of surfactant molecules. We use a chemically-consistent Bayesian modelling of X-ray and neutron reflectometry measurements to show that these monolayers broadly behave as they do on water. This method allows for the monolayer structure to be determined, alongside the molecular volumes of the individual monolayer components without the need for water-specific constraints to be introduced. Furthermore, using this method we are able to better understand the correlations present between parameters in the analytical model. This example of a non-aqueous phospholipid monolayer has important implications for the potential uses of these solvents and for our understanding of how biomolecules behave in the absence of water.

I. INTRODUCTION

Deep eutectic solvents (DES) are green, sustainable liquids that are obtained through the combination of ionic species with compounds that act as hydrogen bond donors, such as sugars, alcohols, amines, and carboxylic acids [1, 2]. The resulting extensive hydrogen bonding network is able to stabilise the ionic species and allows the eutectic mixture to remain liquid at room temperature [3–5]. Through different combinations of the precursor materials, it is possible to tune the solvent's physicochemical properties, such as polarity [6], viscosity and surface tension [1], network charge [7], and hydrophobicity [8, 9]. Recently DES have also been shown to exhibit a "solvophobic" effect through the promotion of surfactant micelle formation [10–13], phospholipid bilayer formation [14–16], and the ability to stabilise non-ionic polymer [17] and protein conformations [18].

Phospholipid monolayers at the air/water interface have been widely studied as simplistic models for biological membranes. As such, they have been used to gain insight into many biological processes that are technologically and medically relevant. For example, investigations at the air/salt-water interface have identified the importance that interactions between charged phospholipid heads and ions present in solution have on the structure, monomer packing and stability of the monolayer [19, 20]. However, the native environment for lipids in-vivo is far from a simple aqueous solution. In fact, it has been suggested [2, 4] that DES might form within the crowded cellular environment and could assist in solubilizing biological species in an intermediate environment between that of the hydrophobic phospholipid tails and highly polar water rich regions, thereby assisting survival under extreme conditions such as freezing temperatures or drought where the water content of cells is restricted.

This work presents the first observation of phospholipid monolayers at an air-DES interface (or for that matter, any ionic solvent, to the best of the authors' knowledge). Furthermore, this is one of very few examples of a phospholipid monolayer at the interface between air and a non-aqueous solvent, with only formamide and mercury being noted previously [21–24]. We have used a chemically-consistent approach to model X-ray (XRR) and neutron (NR) reflectometry measurements and thereby evaluate the effect of this non-aqueous solvent on the structure of phospholipid monolayers.

Recent developments in computational resources and software have enabled powerful methodologies and algorithms to be harnessed by those from non-expert backgrounds. This has benefitted significantly from open-source software projects such as the Python language [25] and the Jupyter notebooks framework [26]. In the area of NR and XRR, the landscape of data-analysis software is diverse, with a range of software packages available

---

[*] A.R.M. and A.S.-F. contributed equally to this work; a.r.mccluskey@bath.ac.uk/andrew.mccluskey@diamond.ac.uk

[†] A.R.M. and A.S.-F. contributed equally to this work; Present address: Department of Food Technology, Lund University, SE-211 00 Lund, Sweden.

[‡] tom.arnold@esss.se

from a variety of sources; refnx [27, 28], MOTOFIT [29], Rascal [30] Aurore [31], Refl1D [32], and GenX [33].

The use of a Python library, such as refnx, enables the implementation custom models that contain chemically-relevant information as well as the application of probability distribution function (PDF) sampling techniques. The Python library emcee [34] offers refnx to access the Goodman & Weare Affine Invariant Markov chain Monte Carlo (MCMC) Ensemble method [35]. This allows the sampling of the high-dimensionality parameter space, relevant in reflectomety analysis, in a Bayesian fashion, where the new samples are generated with consideration of those sampled previously [36]. Bayesian inference gives an understanding of the PDF for the fitted parameters and therefore estimations of their inverse uncertainties and inter-parameter correlations.

II.   EXPERIMENTAL SECTION

A.   Materials

Choline chloride (99 % %, Sigma-Aldrich) and glycerol (99 %, Sigma-Aldrich) d_9-choline chloride (99 %, 98 % D, CK Isotopes) and d_8-glycerol (99 %, 98 % D, CK Isotopes) were purchased and used without further purification. The DES was prepared by mixing the precursors at a 1:2 ratio of chloine chlroide:glycerol, and heating at 80 °C until a homogeneous, transparent liquid formed [1]. The solvent was equilibrated overnight at 40 °C and subsequently stored under a dry atmosphere. Due to the limited availability of the deuterated precursors, a fully protonated subphase (hDES) and a partially deuterated subphase (hdDES) were prepared and used during the neutron reflectometry (NR) experiment. The partially deuterated subphase was prepared using the following mixtures of precursors: 1 mol of 0.38 mol fraction of h-choline chloride/0.62 mol fraction of d-choline chloride; and 2 mol of 0.56 mol fraction of h-glycerol/0.44 mol fraction of d-glycerol. The solvent was subsequently prepared following the procedure discussed above.

The water content of the DES was determined before and after each experiment by Karl-Fischer titration (Mettler Toledo DL32 Karl-Fischer Coulometer, Aqualine Electrolyte A, Aqualine Catholyte CG A) in order to ensure water presence was kept to a minimum. Those measurements showed that the water content of the solvent was kept below 0.3 wt/% during all the experimental procedures presented here, which we assume to be negligible and have to little impact on the characteristics of the DES [3, 4].

1,2-dipalmitoyl-sn-glycero-3-phosphocholine (DPPC, C_{16} tails, >99 %), 1,2-dimyristoyl-sn-glycero-3-phosphocholine (DMPC, C_{14} tails, >99 %), and 1,2-dimyristoyl-sn-glycero-3-phospho-(1'-rac-glycerol) (DMPG, C_{14} tails, >99 %) were supplied by Avanti Polar Lipids and, 2-dilauroyl-sn-glycero-3-phosphocholine (DLPC, C_{12} tails, >99 %) was supplied by Sigma
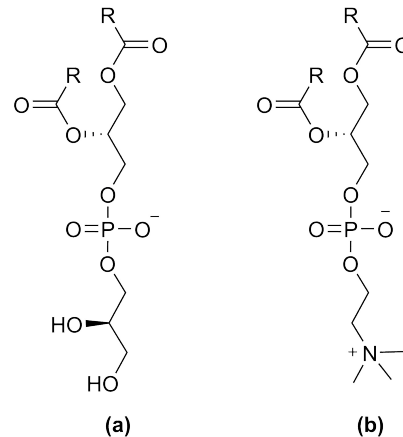

FIG. 1. The two lipid classes with different head groups compared in this study, where R indicates the hydrocarbon tail; (a) phosphatidylglycerol (PG), (b) phosphocholine (PC) [37].

Aldrich and all were used without further purification. Deuterated versions of DPPC (d_{62}-DPPC, >99 %, deuterated tails-only) and DMPC (d_{54}-DPPC, >99 %, deuterated tails-only) were supplied by Avanti Polar Lipids and used without further purification. These phopholipids were dissolved in chloroform (0.5 mg mL^{-1}) at room temperature. PC indicates the molcule contains a phosphocholine head component, where PG contains a phosphatidylglycerol head component, these are shown in Figure 1.

In the XRR experiment, sample preparation was performed in situ using the standard method for the spreading of insoluble monolayers on water: a certain amount of the phospholipid solution was spread onto the liquid surface in order to provide a given surface concentration. After the evaporation of the chloroform, it is assumed that the resulting system is a solvent subphase with a monolayer of phospholipid at the interface. Surface concentration was modified by closing and opening the PTFE barriers of a Langmuir trough. In order to minimise the volumes used in the NR experiment (to keep the cost of deuterated compounds to a manageable level) it was not possible to use a Langmuir trough. Instead, small Delrin adsorption troughs were used that did not have controllable barriers. So, although the surface coverage was nominally the same as used in the X-ray studies, the lack of precise control over the surface pressure meant that it was not appropriate to co-refine XRR and NR contrasts together.

B.   Methods

XRR measurements were taken on I07 at Diamond Light Source, at 12.5 keV photon energy using the double-crystal deflector [38]. The reflected intensity was measured in a momentum transfer range from 0.018 Å^{-1} to 0.7 Å^{-1}. The data were normalised with respect to

the incident beam and the background was measured from off-specular reflection and subsequently subtracted. Samples were equilibrated for at least one hour and preserved under an argon atmosphere to minimise the adsorption of water by the subphase. XRR data were collected for each of the lipids, DLPC, DMPC, DPPC and DMPG at four surface pressures (DLPC: 20, 25, 30 and 35 mN m^{-1}, DMPC: 20, 25, 30 and 40 mN m^{-1}, DPPC: 15, 20, 25 and 30 mN m^{-1}, DMPG: 15, 20, 25 and 30 mN m^{-1}, as measured with an aluminium Wilhelmy plate; all measurements were conducted at 22 °C. The aluminium Wilhelmy plate was used over a traditional paper plate due to the low wetability of paper by the DES.

The NR experiments were performed on FIGARO at the Institut Laue-Langevin using the time-of-flight method [39]. Data at two incident angles of 0.62° and 3.8° were measured to provide a momentum transfer range from 0.005 Å^{-1} to 0.18 Å^{-1}. Two surface pressures for each system and contrast was measured (DMPC: 20 and 25 mN m^{-1}, DPPC: 15 and 20 mN m^{-1}). Similar to the X-ray procedure, samples were given enough time to equilibrate (at least two hours), kept under an inert atmosphere, and all measurements were conducted at 22 °C.

C. Data analysis

The use of XRR and NR to analyse the structure of phospholipids on the surface of water is well documented [19, 20, 40–44]. The models used in the rationalisation of XRR and NR data have varied significantly in numbers of layers present, use of interfactial roughness, and the parameterisation of the physical constraints applied. Frequently, these physical constraints include the volumes of the phospholipid head and tail components, using values taken from other techniques, such as those shown in Table I. Additionally, a recent evaluation of the applicability of different models for surfactant and phospholipid monolayers from the NR perspective has been published [45], that suggests possible oversights in the modelling of NR data.

In Table I, there appears to be a general consensus that the component volume for the phosphocholine (PC) head is around 320 Å^3 to 360 Å^3, while the phosphatidylglycerol (PG) head is in the range 289 Å^3 to 291 Å^3. However, it is not clear is the head component volumes from the literature, that are derived from water-based measurements, will be appropriate for this work, which involves a non-aqueous solvent. The charged nature of the zwitterionic or anionic lipid heads may have different interactions with the polar, but neutral water as compared to the charged DES components [52], which will affect the phospholipid head component volume. Therefore, herein we apply a chemically-consistent model that allows for the co-refinement of reflectometry measurements at different surface pressure, and makes no assumption of the component volume for the lipid head, V_h, or tail, V_t [37]. Instead, these parameters were allowed to vary for each lipid while being constrained to be self-consistent over different surface pressures in the same phase; Liquid-Condensed (LC) for DPPC and Liquid-Expanded (LE) for DMPC, DMPG, and DLPC. Furthermore, it is known that, on water, increase surface pressure and the associated LE-LC phase transitions lead to a compression of the lipid tail volume [53, 54], and this compaction has not necessarily been accounted for in the literature [45]. This model avoids this issue by making no assumption about the molecular volumes and only considers surface pressures that we believe to be in the same phase.

Our chemically-consistent model has been implemented in the Python library refnx [27, 28]. This software allows for the inclusion of a custom model to be defined, from which parameters feed into the Abelès reflectivity model (a model that is widely used to calculate reflectivity [55, 56]). This custom model, along with a series of Jupyter notebooks showing, in full, the analysis performed, can be found in the ESI and is available under a CC BY-SA 4.0 licence [37].

This model consists of two layers to define the lipid monolayer; the head layer at the interface with the solvent and the tail layer at the interface with the air. The head components have a calculated scattering length, b_h, (found as a summation of the X-ray or neutron atomic scattering lengths), and a component volume, V_h. These head components make up a layer with a given thickness, d_h, and roughness, σ_h, within which some volume fraction of solvent can intercalate, ϕ_h. The tail layer is defined in the same fashion, except that the thickness, d_t, is limited such that it may be no greater than the maximum extended length of the lipid tail (the Tanford length, t_t [57]), which is given in Table II, and that no solvent may interacalate into the layer (e.g. $\phi_t = 0$). The scattering length density (SLD) of the tail and head layers used in the Abelès model can therefore be found as follows,

$$\text{SLD}_i = \frac{b_i}{V_i}(1 - \phi_i) + \text{SLD}_s(\phi_i), \qquad (1)$$

where, SLD_s is the scattering length density of the subphase (DES), and i indicates either the tail or head layer. To ensure that the number density of head components and pairs of tail components is the same, the following constraint was included in the model,[58]

$$\phi_h = 1 - \left(\frac{d_t V_h}{V_t d_h}\right). \qquad (2)$$

Based on the work of Campbell et al.,[45] a single value for the interfacial roughness was fitted for all of the interfaces, including the subphase (i.e. $\sigma_h = \sigma_t = \sigma_s$), as there is only a single lipid molecule type in each monolayer. Therefore, any capillary wave roughness at the air-DES interface is carried equally through the layers.

In order to justify the use of a single tail volume across many surface pressures, it was necessary to ensure

TABLE I. Lipid component volumes extracted from different literature sources. V_l corresponds to the total lipid volume, MD to molecular dynamics simulation, WAXS to wide-angle X-ray scattering, NB to neutral buoyancy and DVTD to differential vibrating tube densimetry. [a] The values for the head component in Kucerka *et al.* [46], were taken from Balgavý *et al* [47].

Lipid	DPPC			DMPC		DLPC		DMPG	POPG
Reference	[48]	[49]	[46, 47][a]	[48]]	[46, 47][a]	[48]	[46, 47][a]	[50]	[51]
$V_l/\text{Å}^3$	1287.3 ± 25.5	1148 ± 2	1264.2 ± 32.1	1172.5 ± 25.1	1155.4 ± 30.0	1057.7 ± 24.7	1046.6 ± 28.0	1011.4	1203
$V_t/\text{Å}^3$	966.4 ± 5.4	829 ± 4	924.7 ± 17.6	851.5 ± 5.0	815.9 ± 15.5	736.8 ± 4.6	707.1 ± 13.5	720.4	914
$V_h/\text{Å}^3$	320.9 ± 20.1	319 ± 6	339.5 ± 14.5	320.9 ± 20.1	339.5 ± 14.5	320.9 ± 20.1	339.5 ± 14.5	291.0	289
Method	MD	WAXS	NB	MD	NB	MD	NB	DVTD	MD
T/°C	50	24	30	50	30	50	30	20	25

TABLE II. The invariant parameters within the chemically-consistent model. [a]Values obtained from the Tanford formula [57]. [b]Values obtained from Sanchez-Fernandez *et al.*[10].

Component	b_t/fm	b_h/fm	t_t/Å	SLD/10^{-6}Å^{-2}
X-ray				
DLPC	5073	4674	15.5^a	–
DMPC	5985	4674	18.0^a	–
DPPC	6897	4674	20.5^a	–
DMPG	5985	4731	18.0^a	–
Air	–	–	–	0
DES	–	–	–	10.8^b
Neutron				
d_{54}-DMPC	5329.8	602.7	18.0^a	–
d_{62}-DPPC	6129.2	602.7	20.5^a	–
h-DES	–	–	–	0.43^b
hd-DES	–	–	–	3.15^b

that the lipids remain in the same phase. On water, this can be demonstrated with a Langmuir isotherm. However, while we have confience that the individual surface pressures measured were reliable, we were unable to collect consistent Langmuir isotherm measurements, due to the high viscosity of the DES. Instead we have used grazing incidence X-ray diffraction to confirm the phases of DMPC and DPPC at $30\,\text{mN}\,\text{m}^{-1}$. DPPC was found to be in the LC phase and DMPC in the LE phase at room temperature for the surface pressures measured (see Section S3) [37]. We assume that DMPG and DLPC are also in the LE phase since there is no reason to believe that the phase behaviour in these systems differs significantly from DMPC at the same temperature.

In the first of two steps, this custom model was used to co-refine the component volume of the lipid head component, V_h, the volume of the tail component, V_t, and the head thickness, d_h across XRR measurements at four different surface concentrations. In keeping with the work of Campbell *et al.* [45], a single value for the head thickness was fitted for each lipid across all surface pressures, as the thickness of the head layer was considered to be dependent on molecular dimensions only, and has been shown to vary little with surface pressure [20]. The following parameters were allowed to vary; d_t, and $\sigma_{t,h,s}$, independently across the surface pressures, while others, shown in Table II, were held constant at the values given.

For each co-refinement of four XRR measurements, there were, in total, eleven degrees of freedom in the fitting process. Throughout all of the analysis, the reflectometry scale factor was allowed to vary freely, while the background as constrained to the intensity of either the largest or second-largest q-value.

In the second step, the head and tail component volumes, and head layer thickness determined from XRR were fixed for the refinement of the custom model against the NR measurements. This approach means that the number of variable parameters to fit the NR data can be reduced to two, namely the thickness of the tail layer, d_t, and the interfacial roughness, $\sigma_{t,h,s}$, for the co-refinement of two datasets. Table II also gives the details of the scattering lengths and SLDs used as invariant parameters for the NR fitting.

In both cases, the refinement of the custom model to the experimental data involved the transformation of the reflectometry calculated from the model and the data into Rq^4 such that the contribution of the Fresnel decay was removed, before using the differential evoluation method available to refnx from the scipy library [59], to find the parameters that gave the best fit to the data. The parameter space was then probed using the MCMC method available through emcee [34], which allowed for an estimate of the probability distribution function (PDF) associated with each parameter. In the MCMC sampling, 200 walkers were used over 1000 iterations, following an equilibration of 200 iterations. The use of MCMC sampling allowed for the Bayesian inference of the PDF for each of the variables and their respective interactions. This allowed the Shapiro test to be used to assess if each PDF was normally distributed. Parameters that were shown to be normally distributed are given with symmetric confidence intervals, while those that failed the Shapiro test are given with asymmetric confidence intervals. However, it is important to note that these are not *true* confidence intervals, and account only for the uncertainty present in the data, i.e. they do no account of systematic uncertainty in the measurement that are underrepresented, or unrepresented, in the experimental dataset.
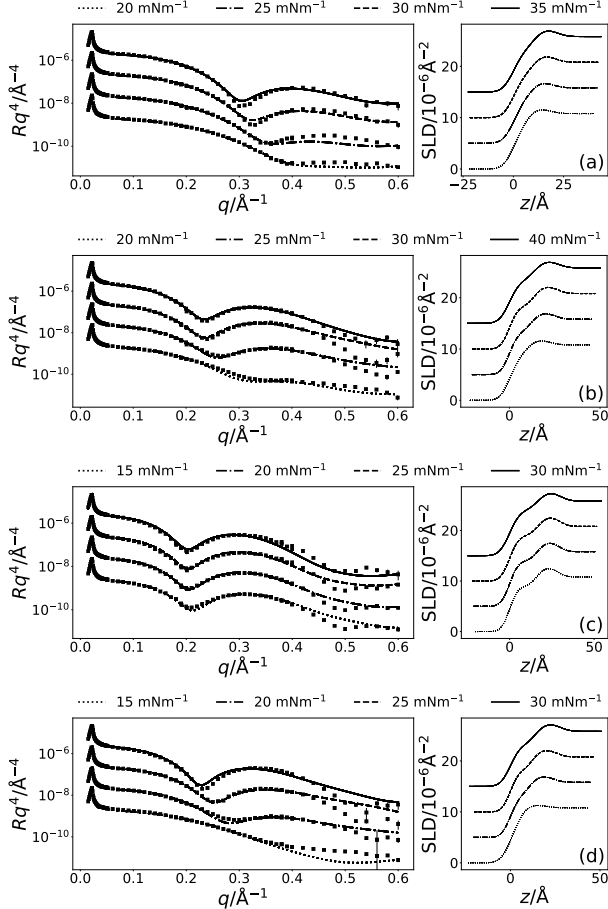
FIG. 2. The XRR profiles (left) and SLD profiles (right) for each of the four lipids; (a) DLPC, (b) DMPC, (c) DPPC, (d) DMPG, at the four measured surface pressures; see legend above each plot. The different surface pressure XRR profiles have been offset in the y-axis by an order of magnitude and SLD profiles offset in the y-axis by 5×10^{-6} Å^{-2}, for clarity [37].
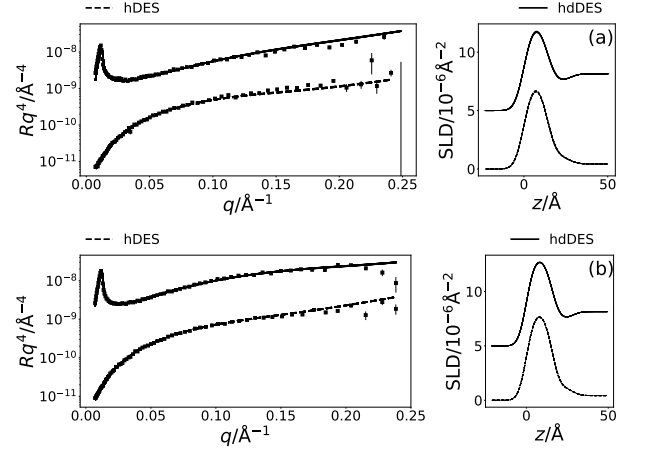

FIG. 3. The NR and SLD profiles at a surface pressure of 20 mNm^{-1} for two contrasts (see legend above each plot); (a) DMPC, (b) DPPC. The NR profiles have been offset in the y-axis by an order of magnitude and SLD profiles offset in the y-axis by 5×10^{-6} Å^{-2}, for clarity [37].

III. RESULTS & DISCUSSIONS

The chemically-consistent model was co-refined across the four surface pressure XRR measurements for each lipid. The resulting XRR profiles and associated SLD profiles are shown in Figure 2. Table III gives details of all varied parameters for each lipid at $30\,\mathrm{mN\,m^{-1}}$, as well as the details of ϕ_h which was determined from Eqn. 2.

Following the initial structural determination of the monolayer by XRR, NR was used to confirm the structure and show the applicability of the chemically-consistent model for DPPC and DMPC. The resulting NR profiles and associated SLD profiles, at a surface pressure of 20 mNm^{-1} are given in Figure 3. Table IV gives details of the varied parameters at each surface pressure as well as ϕ_h as determined from NR.

A. Effect of compression on monolayer thickness

From Tables III and IV, we can see that, as expected and as found in previous work [19, 60], the thickness of the tail layer increases as the number of carbon atoms in the tail chain increases. Furthermore, the thickness of the tail layers in these monolayers appears to agree well with values found for water-analogues; 13.72 ± 0.01 Å at 30 mN/m in DES compared with $d_t = 15.8$Å at $30\,\mathrm{mN\,m^{-1}}$ [41] in water for DMPC, and 16.91 ± 0.01 Å at $30\,\mathrm{mN\,m^{-1}}$ in DES compared with $d_t = 16.7$Å at $40\,\mathrm{mN\,m^{-1}}$ [43] in water for DPPC.

The variation of the tail layer thickness in the models with surface pressure is given for each lipid in Figure 4. It can be observed that as the surface pressure increases, the thickness of the tail layer increases to a point, before plateauing; for DPPC this occurs at $20\,\mathrm{mN\,m^{-1}}$, DMPC at $30\,\mathrm{mN\,m^{-1}}$ and for DMPG and DLPC can be assumed to be at higher pressures than those studied. This phenomenon of the tail thickness increasing with increasing surface pressure has been noted before for DMPC [40] and DPPC [45] at the air-water interface.

B. Effect of compression on solvent concentration

In Figure 4, it is clear that for all four lipids, as the surface pressure is increased there is a corresponding decrease in the percentage solvent present in the lipid head layer. This can be rationalised by considering that when the surface pressure is increased, the free volume available to the solvent between the lipid head components reduces forcing the solvent out of the lipid head layer and into the bulk. A similar effect has been observed when increasing the surface pressure from $11\,\mathrm{mN\,m^{-1}}$ to

TABLE III. The best-fit values, and associated 95 % confidence intervals for the varying parameters in the XRR models, at the $30\,\mathrm{mN\,m^{-1}}$. The values for ϕ_h was obtained from the appropriate use of Eqn. 2 [37].

Lipid	DLPC	DMPC	DPPC	DMPG
$\sigma/\text{Å}$	4.17 ± 0.02	3.86 ± 0.00	4.90 ± 0.00	4.44 ± 0.01
$d_t/\text{Å}$	$9.52^{+0.03}_{-0.04}$	13.72 ± 0.01	16.91 ± 0.01	$13.99^{+0.01}_{-0.01}$
$V_t/\text{Å}^3$	624.92 ± 3.51	718.76 ± 0.52	$765.29^{+0.37}_{-0.38}$	734.01 ± 0.62
$V_h/\text{Å}^3$	331.48 ± 0.58	339.55 ± 0.28	322.01 ± 0.24	$329.95^{+0.32}_{-0.33}$
$d_h/\text{Å}$	$10.98^{+0.13}_{-0.12}$	13.21 ± 0.04	12.69 ± 0.03	13.95 ± 0.04
$\phi_h/\times 10^{-2}$	$54.03^{+1.04}_{-0.95}$	50.93 ± 0.23	43.94 ± 0.22	54.92 ± 0.20

TABLE IV. The best-fit values, and associated 95 % confidence intervals for the varying parameters in the co-refined NR models. The values of ϕ_h were found using Eqn. 2 [37].

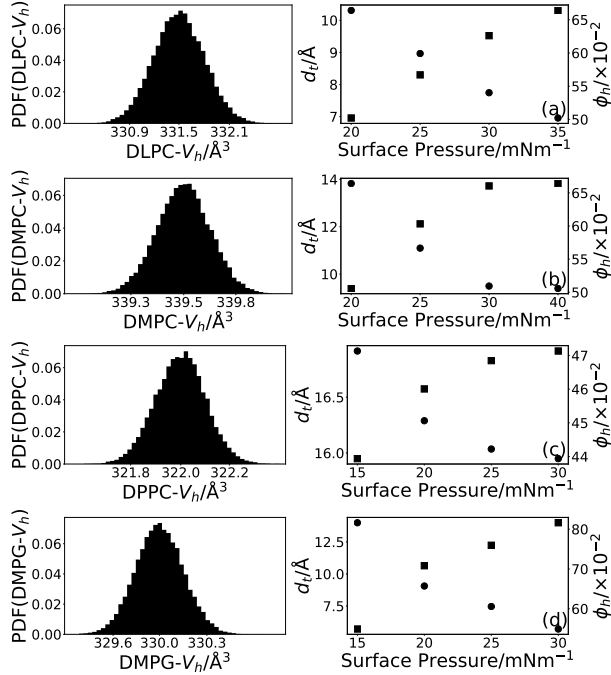| Lipid	d$_{54}$-DMPC		d$_{62}$-DPPC	
SP/mNm^{-1}	20	25	15	20
$\sigma_{t,h,s}/\text{Å}$	4.42 ± 0.16	$3.31^{+0.01}_{-0.02}$	4.27 ± 0.17	3.98 ± 0.10
$d_t/\text{Å}$	13.98 ± 0.15	$17.97^{+0.05}_{-0.01}$	12.32 ± 0.13	15.56 ± 0.10
$\phi_h/\times 10^{-2}$	$50.00^{+0.54}_{-0.54}$	$35.72^{+0.04}_{-0.16}$	$59.16^{+0.43}_{-0.43}$	$48.40^{+0.33}_{-0.33}$

FIG. 4. The PDFs of the head volume (left) and variation of d_t (squares) and ϕ_h (circles) with surface pressure for each of the four lipids; (a) DLPC, (b) DMPC, (c) DPPC, (d) DMPG.

C. Effect of compression on the lipid tail component volumes

It can be seen by comparing Tables I and III that the volume of the lipid tails are significantly lower in the current measurements than found previously, by other techniques. It is unlikely that this is a result of the DES subphase, due to the hydrophobic nature of the lipid tails. However, this reduction has been shown previously [45], where it was rationalised by the compaction of the monolayer at elevated surface pressure. In that work, the optimal value of the tail component volume for DPPC was found to be $772\,\text{Å}^3$ at a surface pressure of $35\,\mathrm{mNm^{-1}}$, this agrees well with the value of $765.29^{+0.37}_{-0.38}$ Å^3 found in this work at surface pressures of 15, 20, 25 and $30\,\mathrm{mN\,m^{-1}}$.

In this work, a single tail component volume was fitted to each lipid for all four surface pressures that were measured. This is based on the assumption, that at all four surface pressures, the lipids adopt the same phase and therefore any variation in the structure with surface pressure would manifest only as a change in the tail thickness. It is clear when comparing Tables I and III that some of the tail component volumes are also reduced in the current XRR measurements compared to those determined previously. The reduction was found to be between 8 % to 12 % for DPPC, DMPC and DLPC when compared with literature sources at $24\,^\circ\text{C}$ to $30\,^\circ\text{C}$, this is in good agreement with the maximum compression percentage of 15 % noted by Small and coworkers [54]. DMPG shows a small increase in the tail volume relative to the literature value quoted at lower temperature. Notably this value is similar to that found in this work for DMPC, which has the same tail structure and suggests that our results are at least self-consistent.

$31\,\mathrm{mN\,m^{-1}}$ for a DMPC/DMPG monolayer at the air-water interface [40].

D. Solvent effect on lipid head component volumes

Figure 4 shows the PDFs determined for the head component volume for each of the four lipids. The three lipids with the PC head component are consistent, giving values of ~ 330 Å^3, regardless of tail component. This agrees well with the values found for the same head component in water, shown in Table I. Interestingly, the component volume for the PG head is similar to that for the PC head with a value of $329.95^{+0.32}_{-0.33}$ Å^3 . The PG head component volume in water, from either DMPG using differential vibrating tube densimetry [50] or POPG using molecular dynamics simulations [51], is noticeably smaller. This indicates that there may be some effect arising from the solvation in choline chloride:glycerol causing an apparent increase in the PG component volume when compared with water. However, as this has only been shown for a single PG-lipid at the air-DES interface.

The major difference between the two head components is the fact PG component is negatively charged whereas the PC component is zwitterionic. It has been shown previously that the conformation for the PC component is folded in water [61], due to the interaction between the positively-charged ammonium and the negatively-charged phosphate groups. A similar structure may occur for the PG component, with the interaction between the partially postively-charged alcoholic hydrogen atoms and the negatively-charged phosphate group. However, such an interaction would be weaker than that observed in the PC component. Therefore, this observed increase found for the PG component volume in DES when compared with water may be due to the unfolding of the PG head. This unfolding would be made possible by the charged nature of the solvent providing a greater screening effect for the PG head than are present in water. This effect may not be observed for the PC component due to the greater strength of the folding arising from the formally-charged nature of the ammonium group. It would be anticipated that this unfolding would result in an increase in the thickness of the lipid head layer. Previously, DPPG has been reported to have a head layer thickness of 10.3(4) Å at 22 mN m^{-1} from neutron reflectometry measurements [42], which it slightly less than the 13.95 ± 0.04 Å determined in the current work, further suggesting that the unfolding of the PG head component may be occurring as a result of interaction with the DES.

E. Refinement of neutron reflectometry

The ability to fit the NR data, as shown in Figure 3 indicates that the values found for the head component volume is consistant between the pair of measurements for the same system. It is clear, that again stable monolayers of the lipids are forming at the air-DES interface, and that the component volumes determined from XRR measurements are robust enough to be used in the mod-
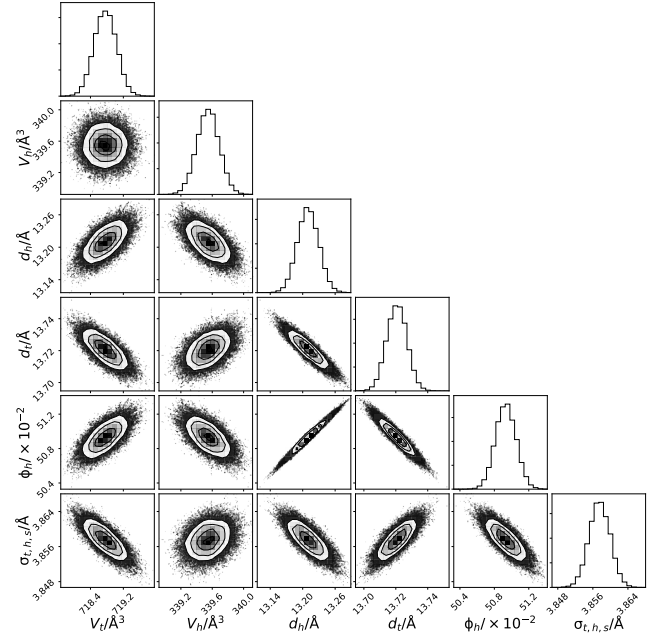

FIG. 5. The multi-parameter PDFs for the chemically-consistent model of DMPC XRR data at 30 mN m^{-1}.

elling of NR data. Futhermore, the trends observed with increasing surface pressure in the XRR models, pertaining to the increasing tail thickness and decreasing solvent concentration in the head components are consistant with that found in the NR models.

F. Interparameter correlations

The use of Bayesian inference and MCMC sampling allowed for the probing of the probability distribution function for each parameter individually. However, it also enables the pairwise interparameter PDFs to be investigated, an example for DMPC at 30 mN m^{-1} is shown in Figure 5 (similar plots for each lipid at each surface pressure measured is available in the ESI [37]). These two-dimensional PDFs give important information about the correlations that are present between the parameters of the chemically-consistant model. The less circular in nature that the 2D PDF is, the greater the correlation that is present between the parameters, e.g. a northeast/south-westerly skewed PDF indicates a positive correlation (where an increase in one parameter correlates an increase in the other) while a north-west/south-easterly skewed PDF indicates a negative correlation (an increase in one correlates with a decrease in the other).

Substantial correlations are present in the parameters fitted to the XRR datasets, indicating important uncertainty that must be considered. In particular, as can be seen in Figure 5, there is a positive correlation between the lipid head thickness, d_h, and the solvent concentra-

tion in the head layer, ϕ_h. This correlation can be rationalised as a result of the SLD of the solvent and the head layer (which is 50 % solvated) being similar, and therefore the boundary between the two is not easy to define. Such a correlations are unavoidable without considering many neutron contrasts of the lipid and solvent, due to the solvophilic nature of the lipid heads. Another, important correlation is that between the head thickness and the tail thickness, d_t, again this is due to the lack of a well defined boundary between the head and tail layers. This is partially driven by the interfacial roughness that is present between the layers, with the correlation being more pronounced for phospholipids with shorted tails (e.g. there is a greater correlation for DLPC than DPPC).

IV. CONCLUSIONS

For the first time, stable phosphocholine and phosphatidylglycerol lipid monolayers have been observed and characterised on a ionic solvent surface. Until the emergence of ionic liquids and DES, only a limited number of molecular solvents exhibited the ability to promote self-assembly and, to the best of our knowledge, only water and formamide among those had demonstrated the formation of phospholipid monolayers at the air-liquid interface.

A physically and chemically constrained modelling approach and Bayesian analysis method was used to rationalise these measurements showing that the structures are remarkably similar at the air-DES interface to those previously observed at the air-water interface. This has the important implication that DES therefore offer the possibility of performing studies of model membranes in the absence of water. Such applications may include fundamental investigations of phospholipid monolayers in extreme environments (total or partial absence of water, cryogenic temperatures), protein membrane interactions and development of new technologies for drug delivery. However, the PG component did show a significant difference; having a larger head component volume than

observed for the same system in water. This suggests that the transfer of lipids to a DES is not just a simple substitution of the subphase. In this specific case we have proposed an explanation based on unfolding of the PG head component that is enabled by electrostatic screening of the component charges by the partially charged solvent. Finally, the use of MCMC sampling of the reflectometry model parameter space give previously unseen insight into the correlations present in XRR data modelling, that should be considered in nature work of this nature.

The ability to determine the head component volume was facilitated by access to easy to use, open-source software that allowed for the straightforward use of a custom, chemically-consistant model within the analysis of the XRR and NR measurements. Futhermore, this work presents the first, to our knowledge, use of chemically-consistant parameterisation to co-refine XRR measurements at different surface concentrations.

V. AUTHOR CONTRIBUTIONS

T.A., A.J.J., A.S.-F. and K.J.E. were involved in the experimental design, and conducted the experiments along with R.A.C.. A.R.M. developed the chemically-consistent model and analysed the data, with input from S.C.P, A.S.-F., T.A., and R.A.C.. A.R.M., A.S.-F. and T.A. wrote the manuscript, with input from all authors.

ACKNOWLEDGMENTS

[1] E. L. Smith, A. P. Abbott, and K. S. Ryder, Chem. Rev. **114**, 11060 (2014).

[2] Y. Dai, J. van Spronsen, G. J. Witkamp, R. Verpoorte, and Y. H. Choi, Anal. Chim. Acta. **766**, 61 (2013).

[3] O. S. Hammond, D. T. Bowron, and K. J. Edler, Green Chem. **18**, 2736 (2016).

[4] O. S. Hammond, D. T. Bowron, A. J. Jackson, T. Arnold, A. Sanchez-Fernandez, N. Tsapataris, V. G. Sakai, and K. J. Edler, J. Phys. Chem. B **121**, 7473 (2017).

[5] C. F. Araujo, J. A. P. Coutinho, M. M. Nolasco, S. F. Parker, P. J. A. Ribeiro-Claro, S. Rudic, B. I. G. Soares, and P. D. Vaz, Phys. Chem. Chem. Phys. **19**, 17998 (2017).

[6] A. Pandey, R. Rai, M. Pal, and S. Pandey, Phys. Chem. Chem. Phys. **16**, 1559 (2014).

[7] S. Zahn, B. Kirchner, and D. Mollenhauer, Chem. Phys. Chem. **17**, 3354 (2016).

[8] B. D. Ribeiro, C. Florindo, L. C. Iff, A. Z. Coelho, and I. M. Marrucho, ACS Sustain. Chem. Eng. **3**, 2469 (2015).

[9] D. J. G. P. van Osch, L. F. Zubeir, A. van der Bruinhorst, M. A. A. Rocha, and M. C. Kroon, Green Chem. **17**, 4518 (2015).

[10] A. Sanchez-Fernandez, T. Arnold, A. J. Jackson, S. L. Fussell, R. K. Heenan, R. A. Campbell, and K. J. Edler, Phys. Chem. Chem. Phys. **18**, 33240 (2016).

[11] T. Arnold, A. J. Jackson, A. Sanchez-Fernandez, D. Magnone, A. E. Terry, and K. J. Edler, Langmuir **31**, 12894 (2015).

[12] Y.-T. Hsieh and Y.-R. Liu, Langmuir **34**, 10270 (2018).

[13] M. K. Banjare, K. Behera, M. L. Satnami, S. Pandey, and K. K. Ghosh, RSC Adv. **8**, 7969 (2018).

[14] S. Bryant, R. Atkin, and G. G. Warr, Langmuir **33**, 6878 (2017).

[15] S. Bryant, R. Atkin, and G. G. Warr, Soft Matter **12**, 1645 (2016).

[16] M. C. Gutiérrez, M. L. Ferrer, C. R. Mateo, and F. del Monte, Langmuir **25**, 5509 (2009).

[17] L. Sapir, C. B. Stanley, and D. Harries, J. Phys. Chem. A **120**, 3253 (2016).

[18] A. Sanchez-Fernandez, K. J. Edler, T. Arnold, D. A. Venero, and A. J. Jackson, Phys. Chem. Chem. Phys. **19**, 8667 (2017).

[19] H. Mohwald, Annu. Rev. Phys. Chem. **41**, 441 (1990).

[20] S. Kewalramani, H. Hlaing, B. M. Ocko, I. Kuzmenko, and M. Fukuto, J. Phys. Chem. Lett. **1**, 489 (2010).

[21] S. P. Weinbach, K. Kjaer, J. Als-Nielsen, M.Lahav, and L. Lieserowitz, J. Phys. Chem. **97**, 5200 (1993).

[22] F. Graner, S. Perez-Oyarzun, A. Saint-Jalmes, C. Flament, and F. Gallet, J. Phys. II France **5**, 313 (1995).

[23] O. M. Magnussen, B. M. Ocko, M. Deutsch, M. J. Regan, P. S. Pershan, D. Abernathy, G. Grübel, and J.-F. Legrand, Nature **384**, 250 (1996).

[24] H. Kraack, B. M. Ocko, P. S. Pershan, E. Sloutskin, and M. Deutsch, Science **298**, 1404 (2002).

[25] G. van Rossum, *Python tutorial, Technical Report CS-R9526*, Tech. Rep. (Centrum voor Wiskunde en Informatica (CWI), 1995).

[26] T. Kluyver, B. Ragan-Kelley, F. Pérez, B. Granger, M. Bussonnier, J. Frederic, K. Kelley, J. Hamrick, J. Grout, S. Corlay, P. Ivanov, D. Avila, S. Abdalla, and C. Willing, in *Positioning and Power in Academic Publishing: Players, Agents and Agendas*, edited by F. Loizides and B. Schmidt (IOS Press, 2016) pp. 87–90.

[27] A. Nelson and S. Prescott, J. Appl. Crystallogr. **52**, xx (2018).

[28] A. Nelson, S. Prescott, I. Gresham, and A. R. McCluskey, "refnx v0.0.17," (2018), available at: `http://doi.org/10.5281/zenodo.1327191`.

[29] A. Nelson, J. Appl. Crystallogr. **39**, 273 (2006).

[30] A. V. Hughes, "Rascal," (2014), available at: `https://sourceforge.net/projects/rscl/`.

[31] Y. Gerelli, J. Appl. Crystallogr. **49**, 330 (2016).

[32] P. A. Kienzle, J. Krycka, N. Patel, and I. Sahin, "Refl1d (version 0.7.9a2)," (2011), available at: `https://refl1d.readthedocs.io/`.

[33] M. Björck and G. Andersson, J. Appl. Crystallogr. **40**, 1174 (2007).

[34] D. Foreman-Mackey, D. W. Hogg, D. Lang, and J. Goodman, Publ. Astron. Soc. Pac. **125**, 306 (2013).

[35] J. Goodman and J. Weare, Comm. App. Math. Comp. Sci. **5**, 65 (2010).

[36] D. S. Sivia and J. Skilling, *Data Analysis: A Bayesian Tutorial*, 2nd ed. (Oxford University Press, Oxford, UK, 2006).

[37] See Supplemental Material at `https://doi.org/10.5281/zenodo.1464836` for details of the chemically-consistent model, information about literature values from measurements on water, grazing incidence X-ray diffraction, and all analysis/plotting scripts and figure files, allowing for a fully reproducible, and automated, analysis workflow.

[38] T. Arnold, C. Nicklin, J. Rawle, J. Sutter, T. Bates, B. Nutter, G. McIntyre, and M. Burt, J. Synchrotron Rad. **19**, 408 (2012).

[39] R. A. Campbell, H. P. Wacklin, I. Sutton, R. Cubitt, and G. Fragneto, Eur. Phys J. Plus **126**, 107 (2011).

[40] T. Bayerl, R. Thomas, J. Penfold, A. Rennie, and E. Sackmann, Biophy. J. **57**, 1095 (1990).

[41] S. J. Johnson, T. M. Bayerl, W. Weihan, H. Noack, J. Penfold, R. K. Thomas, D. Kanellas, A. R. Rennie, and E. Sackmann, Biophys. J. **60**, 1017 (1991).

[42] L. A. Clifton, M. Sanders, C. Kinane, T. Arnold, K. J. Edler, C. Neylon, R. J. Green, and R. A. Frazier, Phys. Chem. Chem. Phys. **14**, 13569 (2012).

[43] C. A. Helm, H. Möhwald, K. Kjær, and J. Als-Nielsen, EPL **4**, 697 (1987).

[44] J. Daillant, L. Bosio, and J. J. Benattar, EPL **12**, 715 (1990).

[45] R. A. Campbell, Y. Saaka, Y. Shao, Y. Gerelli, R. Cubitt, E. Nazaruk, D. Matyszewska, and M. J. Lawrence, J. Colloid Interface Sci. **531**, 98 (2018).

[46] N. Kučerka, M. A. Kiselev, and P. Balgavý, Eur. Biophys. J. **33**, 328 (2004).

[47] P. Balgavý, N. Kučerka, V. I. Gordeliy, and V. G. Cherezov, Acta Phys. Solvaca **51**, 53 (2001).

[48] R. S. Armen, O. D. Uitto, and S. E. Feller, Biophys. J. **75**, 734 (1998).

[49] W. J. Sun, R. M. Suter, M. A. Knewtson, C. R. Worthington, S. Tristram-Nagle, R. Zhang, and J. F. Nagle, Phys. Rev. E **49**, 4665 (1994).

[50] J. Pan, F. A. Heberle, S. Tristram-Nagle, M. Szymanski, M. Koepfinger, J. Katsaras, and N. Kučerka, BBA - Biomembranes **1818**, 2135 (2012).

[51] N. Kučerka, B. W. Holland, C. G. Gray, B. Tomberli, and J. Katsaras, J. Phys. Chem. B **116**, 232 (2012).

[52] A. Sanchez-Fernandez, G. L. Moody, L. C. Murfin, T. Arnold, A. J. Jackson, S. M. King, S. E. Lewis, and K. J. Edler, Soft Matter **14**, 5525 (2018).

[53] D. Marsh, Chem. Phys. Lipids **163**, 667 (2010).

[54] D. M. Small, J. Lipid Res. **25**, 1490 (1984).

[55] F. Abelès, J. Phys. Radium **11**, 307 (1950).

[56] L. G. Parratt, Phys. Rev. **95**, 359 (1954).

[57] C. Tanford, *The Hydrophobic Effect: Formation of Micelles and Biological Membranes*, 2nd ed. (John Wiley & Sons Ltd., Somerset, NJ, USA, 1980).

[58] L. Braun, M. Uhlig, R. von Klitzing, and R. A. Campbell, Adv. Colloid Interface Sci **247**, 130 (2017).

[59] E. Jones, T. Oliphant, P. Peterson, *et al.*, "SciPy: Open source scientific tools for Python," (2001), available at: `http://www.scipy.org/`.

[60] D. Vaknin, K. Kjaer, J. Als-Nielsen, and M. Lösche, Biophys. J. **59**, 1325 (1991).

[61] R. J. Gillams, C. D. Lorenz, and S. E. McLain, J. Chem. Phys. **144**, 225101 (2016).